Geophysical Research Letters

Supporting Information for

Complexity in the evolution, composition, and spectroscopy of brown carbon in aircraft measurements of wildfire plumes

R. A. Washenfelder[1], L. Azzarello[2], K. Ball[1,3,a], S. S. Brown[1,4], Z. C. J. Decker[1,4,5], A. Franchin[1,5,b], C. D. Fredrickson[6], K. Hayden[7], C. D. Holmes[8], A. M. Middlebrook[1], B. B. Palm[6,b], R. B. Pierce[9], D. J. Price[1,5], J. M. Roberts[1], M. A. Robinson[1,4,5], J. A. Thornton[6], C. C. Womack[1,5], C. J. Young[2]

[1]Chemical Sciences Laboratory, National Oceanic and Atmospheric Administration, 325 Broadway, Boulder, CO 80305, USA

[2]Department of Chemistry, York University, Toronto, ON, Canada

[3]University of Maryland Baltimore County, Baltimore, MD 21250, USA

[4]Department of Chemistry, University of Colorado, Boulder, CO 80309, USA

[5]Cooperative Institute for Research in Environmental Sciences, University of Colorado, Boulder, CO 80309, USA

[6]Department of Atmospheric Sciences, University of Washington, Seattle, WA 98195, USA

[7]Air Quality Research Division, Environment and Climate Change Canada, Toronto, ON, Canada, M3H 5T4

[8]Earth, Ocean, and Atmospheric Science, Florida State University, Tallahassee, FL 32304, USA

[9]Space Science and Engineering Center, University of Wisconsin, Madison, WI 53706, USA

[a]Now at: Division of Chemistry and Chemical Engineering, California Institute of Technology, Pasadena, CA 91125, USA

[b]Now at: National Center for Atmospheric Research, Boulder, CO 80307, USA

Contents of this file

Text S1.

Description of shared aerosol inlet

The aerosol instruments sampled from a forward-facing, near-isokinetic inlet [*Schwarz et al.*, 2006; *Perring et al.*, 2013]. For flights from 9 Aug 2019 onward, the aerosol flow was actively pressure-controlled at 620 hPa using a flow restriction (0.21 cm inner diameter, 3.1 cm length), pressure controller (PCP-15PSIA-D-DB15; Alicat Scientific Inc, Tucson, AZ, USA), and scroll pump (IDP-3; Agilent, Santa Clara, CA, USA). The total inlet flow of 8.13 slpm passed through an impactor (TE296, Tisch Environmental, Cleves, OH, USA) with a measured 50% cutpoint at 0.95 μm, before being distributed to the aerosol instruments through a series of y-shaped splitters.

Description of BrC-PILS Instrument

The incoming aerosol flow to the BrC-PILS instrument was sampled through an automated valve (MDM-060DT; Hanbay Laboratory Automation, Pointe Claire, QC, Canada) with filter (116IL; Headline Filters Limited, Aylesford, Kent, England) for periodic, automated measurements of the aerosol-free background. The flow was maintained at a constant 6.0 standard L min^{-1} (slpm) using a 1.35 mm diameter critical orifice (Lenox Laser, Glen Arm, MD, USA) between the PILS and the scroll pump. A parallel-plate carbon filter denuder (DN-100; Sunset Laboratory, Tigard, OR, USA) removed gas-phase VOCs. A pressure sensor (PPT; Honeywell Inc., Plymouth, MN, USA) measured the upstream pressure. The particle-into-liquid sampler collected aerosol in solution using a steam generator and droplet impactor (PILS 4001; Brechtel Manufacturing Inc., Hayward, CA, USA), with an average output liquid sample flow of 1.53 mL min^{-1}. Bubbles were removed from the liquid sample stream using a flow-through debubbler consisting of a porous polytetrafluoroethylene (PTFE) membrane under vacuum (Omnifit 006BT; Diba Industries, Inc., Danbury, CT modified by Brechtel Manufacturing Inc.). Insoluble components were removed from the liquid sample stream using a particle filter (Puradisc 25 TF; GE Healthcare Life Sciences, Pittsburgh, PA, USA). The liquid flowed into a 2.5 m liquid waveguide capillary cell (LWCC-3250; World Precision Instruments, Sarasota, FL, USA). A 1.1 mL min^{-1} flow was then sampled by a TOC analyzer (M9 Portable TOC Analyzer; GE

Analytical Instruments Inc., Boulder, CO, USA) for measurement of water-soluble organic carbon (WSOC). The excess flow (~0.43 mL min^{-1}) was directed by an automated 14-port valve (C25Z; Vici Valco Instruments, Houston, TX, USA) to a series of 12 polypropylene sample tubes for offline analysis or to a waste container. All of the liquid flow system components consisted of PTFE and polyetheretherketone (PEEK) tubing and fittings.

The BrC-PILS optical system consisted of a deuterium/halogen light source with spectral output from 200–2500 nm (DH-mini; Ocean Optics Inc., Dunedin, FL, USA) coupled to the liquid waveguide capillary cell. The exiting light was coupled to a 101 mm focal length symmetrical cross Czerny-Turner spectrometer with an 18-bit back-thinned 1024 × 58 pixel CCD array detector cooled to -5 deg C (QE Pro; Ocean Optics Inc., Dunedin, FL, USA). The spectrometer contains a 600 groove mm^{-1} grating (300 nm blaze wavelength) rotated to give a useful spectral range from 309 to 682 nm and spectral resolution of 0.36 nm. The entrance slit is 200 μm wide × 1000 μm tall, and is illuminated by a fiber bundle containing a linear array of 200 μm diameter UV/Vis fibers. Fifty spectra with 0.02 s integration time were averaged to 1 Hz. Both the BrC-PILS absorption and WSOC concentrations were corrected by a factor of 1.25 to account for the measured collection efficiency of the PILS under these operating conditions. This correction factor was determined in the laboratory by introducing aerosolized sucrose to the BrC-PILS through the pressure-controlled inlet and comparing the measured WSOC concentrations to expected values from size distributions measured by an optical particle counter. We follow the method of *Hecobian et al.* [2010] to calculate absorption and WSOC using the liquid and gas flows, as described below. We report water-soluble absorption in units of Mm^{-1}. The measurements are presented as absorbance in solution, without the Mie correction for aerosol absorbance. We report WSOC concentration in units of μg C std m^{-3}.

Although the BrC-PILS instrument reports absorption at 1 Hz and WSOC at 0.25 Hz, the absorption signal is effectively smoothed by 60 s and the WSOC signal is effectively smoothed by 120 s due to the time response of the water collection and measurement. For calculations that compare the BrC-PILS data to coincident aircraft

measurements with true 1 Hz time response, those datasets are convolved with a 60-s or 120-s boxcar.

Calculation of aerosol absorption

Solution absorption was calculated from Beer's Law:

$$\alpha_{solution}(\lambda) = c_{solution} \cdot \sigma_{solution}(\lambda) = \frac{1}{l} \cdot log_{10}\left(\frac{I_0}{I}\right) \quad \text{(S1)}$$

where $\alpha_{solution}$ is absorption coefficient of the solution, λ is wavelength, c is concentration, $\sigma_{solution}$ is the mass absorption efficiency, l is the LWCC cell length, I_0 is light intensity in the absence of the absorber, and I is light intensity with the absorber present. This was converted to an absorption coefficient for the aerosol:

$$\alpha_{aerosol}(\lambda) = \alpha_{solution}(\lambda) \cdot \frac{V_{solution}}{V_{gas}} \cdot \ln(10) \cdot M(\lambda) \quad \text{(S2)}$$

where $\alpha_{aerosol}$ is the absorption, $V_{solution}$ is the PILS liquid sample flow rate (1.53 mL min^{-1}), V_{gas} is the PILS gas flow rate (6.0 slpm), and $M(\lambda)$ is a correction for Mie effects between the solution and aerosol that was not applied for this work.

Nitroaromatic absorption cross-sections and pH

Nitroaromatics may exist in protonated or deprotonated forms with different absorption cross-sections, depending on the solution pH and their pKa. We measured an average pH value of 5±1 for four aqueous samples collected in three smoke plumes by the BrC-PILS. At this pH, 2 nitrophenol, 4-nitrophenol, 4-nitrocatechol, and 4 nitroguaiacal are predominantly protonated (pKa values of 7.14, 7.23, 6.87, and 7.05 respectively), while 2,4 dinitrophenol is predominantly deprotonated (pKa 4.04) [Hinrichs et al., 2016], as shown in Fig 4c. The absorption spectrum of protonated 4-nitrocatechol from *Hinrichs et al. [2016]* was confirmed using liquid waveguide capillary cell measurements of pure 4-nitrocatechol in water, which showed an average agreement of 4.5% at 315–415 nm.

Spectral fitting using modeled ratios of nitroaromatic concentrations

In addition to fitting individual absorbers, we calculated a weighted absorption cross-section from the modeled ratio of nitroaromatic concentrations after 1.3 h of daytime transport, as described in *Robinson et al.* [2021]. The weighted cross-section is equal to $0.5\times\sigma_{4\text{-nitrocatechol}} + 0.3\times\sigma_{4\text{-nitroguaiacol}} + 0.2\times\sigma_{2\text{-nitrophenol}}$ with no contribution predicted from 2,4-dinitrophenol or 2-nitrophenol. Fits with the weighted cross-section and power law (Eqn. 3), show that the contribution of nitroaromatic compounds to the total absorption is <1.1% at 365 nm and <0.5% at 405 nm.

Description of the UHSAS and AMS instruments

The Ultra-High Sensitivity Aerosol Spectrometer (UHSAS; Droplet Measurement Technologies, Longmont, CO, USA) and the Aerosol Mass Spectrometer (AMS; Aerodyne Research Inc., Billerica, MA, USA) instruments sampled from the shared, pressure-controlled aerosol inlet, using a y-splitter (Brechtel Manufacturing Inc., Hayward, CA, USA).

The UHSAS sample flow was diluted by filtering a portion of its total flow with a high-efficiency particle filter (Pall Corporation, Port Washington, NY, USA) when aerosol number concentrations were greater than ~1000 cm^{-3}, to minimize coincident particle detections [*Kupc et al.*, 2018]. The filtered and unfiltered flow were measured using laminar flow elements, and used to correct the particle concentration measurements. The UHSAS calibration was periodically checked with monodisperse ammonium sulfate particles generated with a custom atomizer and differential mobility analyzer.

The flow for the high-resolution, time-of-flight aerosol mass spectrometer (HR-ToF-AMS) [*DeCarlo et al.*, 2006; *Liggio et al.*, 2016] was picked off with a pseudo isokinetic core-sampling tube, with the remainder of the sampling line going to a filter-based continuous light absorption photometer [*Ogren et al.*, 2017]. The AMS sampled in Fast Mass Spectrometry (FMS) mode [*Kimmel et al.*, 2011], where 1 s average mass spectra were recorded while cycling repeated blocks of 3 s with the chopper closed, 39 s with the chopper open, and 3 s again with the chopper closed. To capture sub-plume-scale heterogeneity, we sampled solely in FMS mode and did not measure aerosol mass size distributions. The high-resolution AMS spectra were analyzed with open source Igor

Pro (Wavemetrics, Lake Oswego, OR, USA) software packages: ToF-AMS Analysis Toolkit SQUIRREL V.1.63 and ToF-AMS HR Analysis PIKA v. 1.23.

The AMS nitrate ionization efficiency was calibrated periodically with ammonium nitrate particles using the methodology described in the SI material of *Franchin et al.* [2018]. The nitrate relative ionization efficiency (RIE) is 1.05, based on the default fragmentation table. Ammonium nitrate calibrations were used to determine the RIE for ammonium and default RIE values were used for the other standard AMS species (1.4 for organics, 1.2 for sulfate, and 1.3 for chloride). In the absence of direct, in-situ comparisons onboard the FIREX-AQ Chemistry Twin Otter, a collection efficiency (CE) of 0.5 was used for all species. This is based on a field campaign with some in-situ observations of biomass burning aerosols with a compact-Time-of-Flight AMS instrument equipped with a light scattering module (LS-C-ToF AMS) for an independent measurement of CE [*Liao et al.*, 2017]. The average oxygen-to-carbon mole ratios were determined using the "Improved-Ambient" method in the PIKA data analysis package [*Canagaratna et al.*, 2015]. Reported oxygen-to-carbon ratios were constrained between zero (methane) and two (oxalic acid).

Description of the 4-nitrocatechol mass calibration

The AMS tracer ions for 4-nitrocatechol ($C_6H_5NO_3^+$ at m/z = 139.026901 and $C_6H_5NO_4^+$ at m/z = 155.021896) were fit from the high resolution (HR) spectra assuming that there were no interfering signals at $C_7H_7O_3^+$ (m/z = 139.039505) and $C_7H_7O^{4+}$ (m/z = 155.034393), which the HR-ToF-AMS could not resolve separately from the tracer ions. For the laboratory data, the contribution of m/z 139 ($C_6H_5NO_3^+$) to the sum of the two tracer ions (m/z 139 + m/z 155; $C_6H_5NO_3^+$ + $C_6H_5NO_4^+$) was 5.5% ± 2.0%, regardless of spectral mass resolution (HR-ToF-AMS or LS-C-ToF AMS). This indicates that mass spectra of pure 4-nitrocatechol particles have significantly more signal from the parent ion than from the ion fragment with one less oxygen atom. In contrast, for the FIREX-AQ field measurements, the contribution of $C_6H_5NO_3^+$ to the sum of the tracer ions ($C_6H_5NO_3^+$ + $C_6H_5NO_4^+$) averaged 67% ± 17%. It is possible that the difference in ion ratios is due to increased interference from other species in the ambient smoke spectra.

The mass concentrations (in units of μg std m^{-3}) for these tracer ions were calculated using CE = 0.5 (same as all species) and RIE = 1.4 (same as organics). These tracer ions were calibrated using pure 4-nitrocatechol (Sigma Aldrich, ≥96% purity) aerosol particles that were generated from aqueous solutions, dried and diluted with zero air, and size-selected with a centrifugal particle mass analyzer (CPMA; Cambustion Ltd., Cambridge, UK). Particle sizes were measured with the UHSAS and the volume fraction of particles transmitted into the AMS with a standard lens [*Liu et al.*, 2007] was calculated for each data set. The CPMA diameters were selected from 200 to 350 nm with multiply-charged larger modes, and the calculated fraction transmitted into the AMS decreased from 97% to 77%, respectively. The absolute mass concentration of 4-nitrocatechol sampled by the AMS was measured directly with a catalyst-based total particulate nitrogen technique [*Stockwell et al.*, 2018].

The shared sampling line included denuders to remove gas phase acids, bases, and organic species and the resulting particles were sampled directly into the hot catalyst and the other aerosol instruments. The platinum and molybdenum catalyst system converted the remaining particulate nitrogen from a variety of compounds into detectable gas phase nitrogen oxide. After correcting the total particulate nitrogen measurement to account for the AMS lens transmission losses discussed above, the total particulate nitrogen from the catalyst system and measured ammonium nitrate from the AMS were nearly identical, indicating complete conversion of particulate nitrate into gaseous nitrogen oxide.

There were no observed interferences by other species during the pure 4-nitrocatechol experiments, so unit mass tracer ion peaks at m/z 139 and 155 were sufficient for the calibrations. These calibrations were performed over multiple days using the same HR-ToF AMS instrument that was used on the FIREX-AQ Chemistry Twin Otter aircraft as well as with the unit-mass-resolution LS-C-ToF AMS instrument. The average collection efficiency of pure 4-nitrocatechol particles measured by the light scattering AMS was 0.5 ± 0.2. For the purposes of this paper, only the ratio of the absolute 4-nitrocatechol mass concentrations from the total particulate nitrogen

technique to the mass concentrations of the AMS tracer ions using the same CE and RIE as the field data were needed. This assumes that the CE and RIE for 4-nitrocatechol were the same for the pure calibration particles and the wildfire smoke. The linear correlation between 4-nitrocatechol and the AMS tracer ion sum (m/z 139 + m/z 155) from four separate calibration days (n=233) shown in Fig. S2 was (15.8 ± 0.1) × (m/z 139 + m/z 155) μg std m^{-3}. The calibrations are linear over more than two orders of magnitude (Fig. S2).

Comparison of the 4-nitrocatechol mass calibration in this work and *Palm et al.* [2020]

The calibration for pure 4-nitrocatechol (Fig. S2) determined here is lower than that reported by *Palm et al.* [2020]. The major difference between these two calibrations is the determination of nitrophenol mass concentrations. The current calibration uses an absolute gas-phase standard based on the aerosol nitrogen content [*Stockwell et al.*, 2018]. In contrast, the calibration data shown in Fig. 5a of *Palm et al. [2020]* were determined from chamber experiments of oxidized phenol and catechol, with the resulting particulate nitrophenol and nitrocatechol detected by HR-ToF-AMS and Filter Inlet for Gases and AEROsols (FIGAERO) I^- CIMS. The FIGAERO inlet collects particles directly onto a 24 mm diameter Zefluor® PTFE filter (Pall Corporation, Port Washington, NY, USA) with a typical aerosol retention of over 99.99%. The two calibration slopes for the AMS tracer ions indicate that the FIGAERO I^- CIMS measures over a factor of four greater mass of nitrophenols than the total particulate nitrogen technique. Two possible explanations for the discrepancy are AMS lens transmission and AMS collection efficiency, which are discussed in detail below.

The first possible explanation for the difference in calibration slopes is that particles deposited onto the FIGAERO inlet filter were too large to be quantitatively transmitted through the AMS sampling lens. The Monoterpene and Oxygenated aromatics Oxidation at Night and under LIGHTs (MOONLIGHT) experiments described in *Palm et al.* [2020] used large concentrations of ammonium sulfate seed particles (~150 μg m^{-3}). AMS lens transmission losses could be exacerbated as the seed particles grow

after condensation, especially since the apparent increase in mass concentrations for these experiments was as much as 100 μg m^{-3} (Figs. 5a and S8 of *Palm et al.*). Data points for <10 μg m^{-3} of phenolic compounds in Fig. 5a of *Palm et al.* [2020] appear to have a slope that is close to the -50% bound of the calibration line, indicating a change in sensitivity between high and low mass concentrations. Possible differences in particle size sampling between the AMS and FIGAERO CIMS I^- during MOONLIGHT are discussed in the SI material of *Garofalo et al.* [2021]. In contrast, for this work the calibration data shown in Fig. S2 were corrected for the calculated standard lens transmission losses and are linear over more than two orders of magnitude, indicating that the AMS sensitivity did not change for a range of concentrations and selected sizes in the calibration plot.

The second possible explanation for the difference in calibration slopes is AMS collection efficiency (CE). The CE value used in determining the AMS tracer ion mass concentrations is an important factor in both sets of calibration experiments. For the 4-nitrocatechol calibrations here, we measured and used a CE value of 0.5. For the MOONLIGHT data in *Palm et al.* [2020], CE = 0.65 was used. However, most of the oxidation products condensed onto dry ammonium sulfate seed particles [*Garafalo et al.,* 2021] that have a CE ~ 0.25 [*Matthew et al.*, 2008]. For previous experiments where dry ammonium sulfate particles were coated with an organic liquid compound, mass fractions larger than 0.5 were needed before the CE value represented the liquid value [*Matthew et al.*, 2008]. The amount of material condensed in the MOONLIGHT calibrations appears to be lower than this, such that a CE value lower than 0.65 should likely be used in determining the AMS tracer ion mass concentrations for the calibrations. Furthermore, it is possible that the CE was not consistent for all of the MOONLIGHT experiments as the amount of oxidation products on the sulfate seeds increased over time and varied between experiments [*Garafalo et al.*, 2021]. Thus the slope of the calibration plot in Fig. 5a for the *Palm et al.* work is potentially high by as much as a factor of 2.6 (=0.65/0.25).

References

Canagaratna, M. R., et al. (2015), Elemental ratio measurements of organic compounds using aerosol mass spectrometry: Characterization, improved calibration, and implications, *Atmos. Chem. Phys.*, *15*(1), 253-272.

DeCarlo, P. F., et al. (2006), Field-deployable, high-resolution, time-of-flight aerosol mass spectrometer, *Anal. Chem.*, *78*(24), 8281-8289.

Franchin, A., et al. (2018), Airborne and ground-based observations of ammonium-nitrate-dominated aerosols in a shallow boundary layer during intense winter pollution episodes in northern Utah, *Atmos. Chem. Phys.*, *18*(23), 17259-17276.

Garofalo, L. A., et al. (2021), Heterogeneous nucleation drives particle size segregation in sequential ozone and nitrate radical oxidation of catechol, *Environ. Sci. Technol.*, *55*(23), 15637-15645.

Hecobian, A., et al. (2010), Water-soluble organic aerosol material and the light-absorption characteristics of aqueous extracts measured over the Southeastern United States, *Atmos. Chem. Phys.*, *10*(13), 5965-5977.

Hinrichs, R. Z., et al. (2016), Solar absorption by aerosol-bound nitrophenols compared to aqueous and gaseous nitrophenols, *Environ. Sci. Technol.*, *50*(11), 5661-5667.

Kimmel, J. R., et al. (2011), Real-time aerosol mass spectrometry with millisecond resolution, *Int. J. Mass Spectrom.*, *303*(1), 15-26.

Kupc, A., et al. (2018), Modification, calibration, and performance of the Ultra-High Sensitivity Aerosol Spectrometer for particle size distribution and volatility measurements during the Atmospheric Tomography Mission (ATom) airborne campaign, *Atmos. Meas. Tech.*, *11*(1), 369-383.

Liao, J., et al. (2017), Single-particle measurements of bouncing particles and in situ collection efficiency from an airborne aerosol mass spectrometer (AMS) with light-scattering detection, *Atmos. Meas. Tech.*, *10*(10), 3801-3820.

Liggio, J., et al. (2016), Oil sands operations as a large source of secondary organic aerosols, *Nature*, *534*(7605), 91-94.

Liu, P. S. K., et al. (2007), Transmission efficiency of an aerodynamic focusing lens system: Comparison of model calculations and laboratory measurements for the Aerodyne Aerosol Mass Spectrometer, *Aerosol Sci. Tech.*, *41*(8), 721-733.

Matthew, B. M., et al. (2008), Collection Efficiencies in an Aerodyne Aerosol Mass Spectrometer as a Function of Particle Phase for Laboratory Generated Aerosols, *Aerosol Sci. Tech.*, *42*(11), 884-898.

Ogren, J. A., et al. (2017), Continuous light absorption photometer for long-term studies, *Atmos. Meas. Tech.*, *10*(12), 4805-4818.

Palm, B. B., et al. (2020), Quantification of organic aerosol and brown carbon evolution in fresh wildfire plumes, *Proc. Natl. Acad. Sci. USA*, *117*(47), 29469-29477.

Perring, A. E., et al. (2013), Evaluation of a perpendicular inlet for airborne sampling of interstitial submicron black-carbon aerosol, *Aerosol Sci. Tech.*, *47*(10), 1066-1072.

Robinson, M. A., et al. (2021), Variability and time of day dependence of ozone photochemistry in western wildfire plumes, *Environ. Sci. Technol.*, *55*(15), 10280-10290.

Schwarz, J. P., et al. (2006), Single-particle measurements of midlatitude black carbon and light-scattering aerosols from the boundary layer to the lower stratosphere, *J. Geophys. Res.-Atmos.*, *111*, D16207.

Stockwell, C. E., et al. (2018), Characterization of a catalyst-based conversion technique to measure total particulate nitrogen and organic carbon and comparison to a particle mass measurement instrument, *Atmos. Meas. Tech.*, *11*(5), 2749-2768.

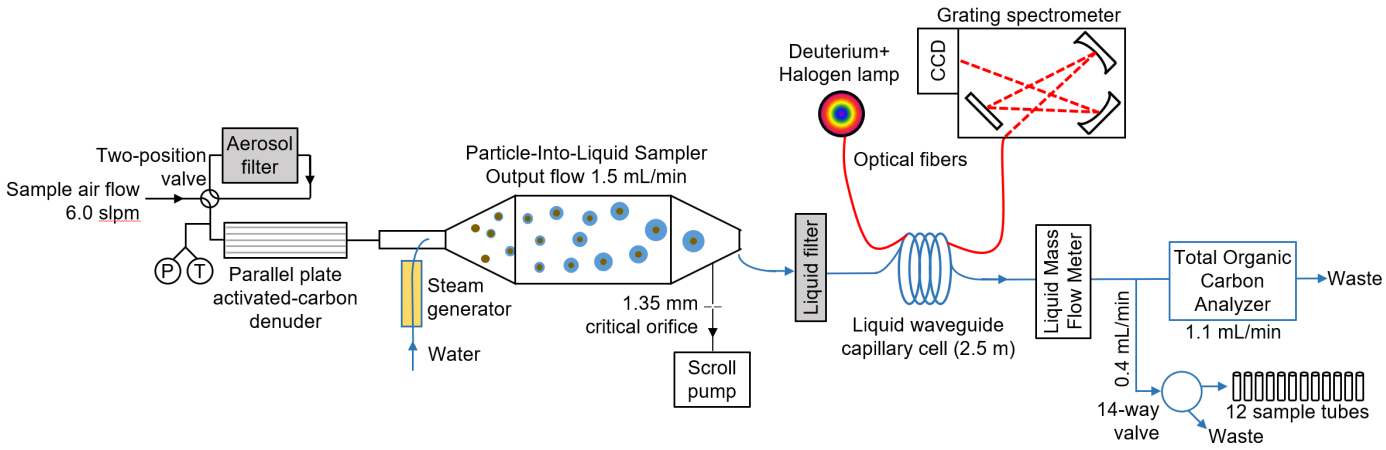

Figure S1. Schematic of the BrC-PILS instrument on the NOAA Twin Otter during the FIREX-AQ 2019 field campaign. P and T represent pressure and temperature sensors.

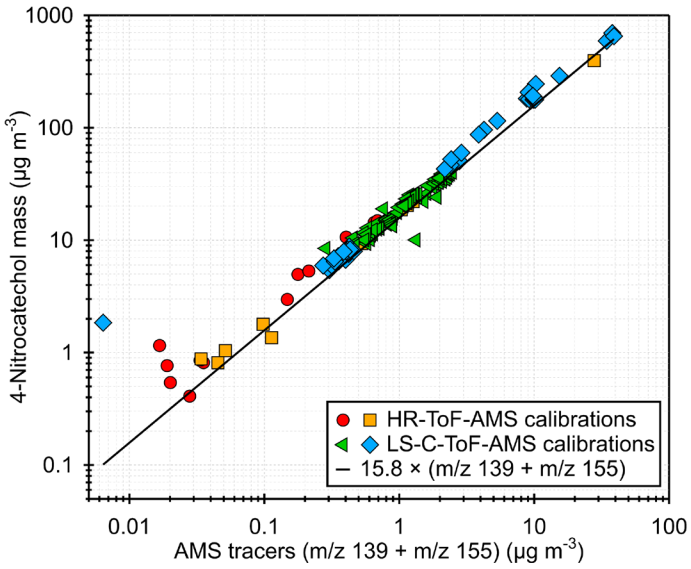

Figure S2. Comparison of aerosolized 4-nitrocatechol mass measured by the total particulate nitrogen instrument and AMS (m/z 139 + m/z 155). The colored symbols show four calibration experiments with the HR-ToF-AMS or LS-C-ToF-AMS. The black line is the average calibration ratio from the experiments.

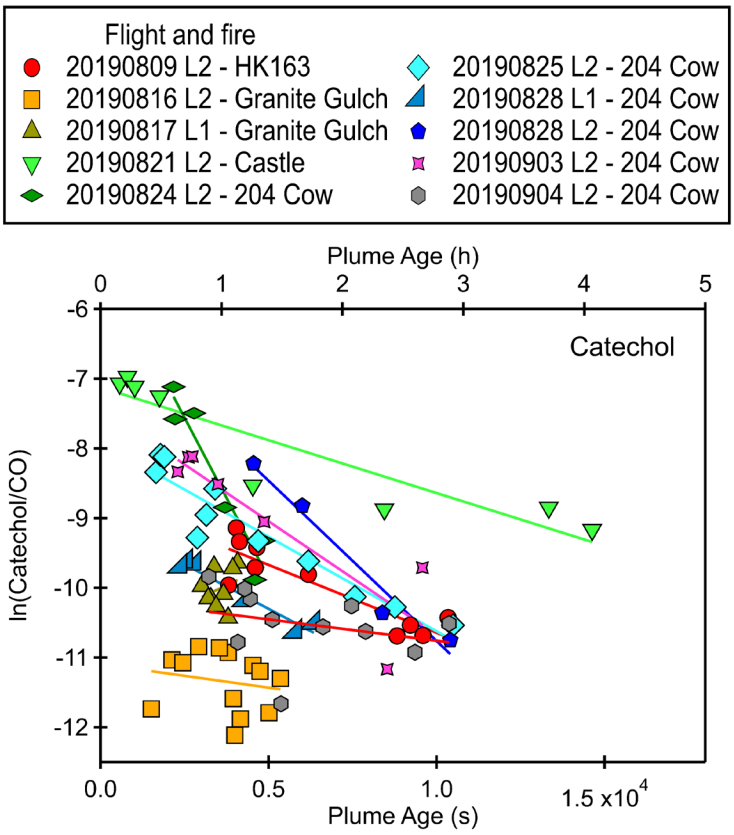

Figure S3. The trend in ln(catechol/CO) vs reanalysis plume age shows rapid loss of gas-phase catechol due to its daytime reaction with OH. Each color and symbol represent a different flight leg and each point represents a single plume transect. Secondary formation of catechol from the reaction of phenol with OH contributes uncertainty to the chemical plume age calculations, but catechol was selected due to its rapid reaction with OH.